



# Finite-element simulation and validation of material flow in thermal drilling process

R. Kumar<sup>1</sup> · N. Rajesh Jesudoss Hynes<sup>1</sup>

Received: 1 June 2017 / Accepted: 3 October 2017 / Published online: 27 February 2018  
© The Brazilian Society of Mechanical Sciences and Engineering 2018

## Abstract

Galvanized steel is broadly employed in metal roofing, air conditioning duct, support beams, construction materials, and domestic appliances, etc. In conventional drilling method has limitations such as asymmetrical holes, as well as formation of crack inside the hole made in sheet metal. This problem was entirely exterminated in thermal drilling (TD) process. In the course of TD process, the high temperature was developed due to rotational and feed rate of thermal drill into the workpiece. Owing to this reason, the thermal drill pierces workpiece effortlessly. However, in this process, workpiece deformation is very high; therefore, finite-element simulation is used to study the material flow which is challenging in experimental method. According to finite-element method (FEM), the finite-element analysis of TD process was conducted by the DEFORM-3D simulation software. The aim of this study is to conduct an experimental investigation of TD process on galvanized steel (GS), and then, it is compared to numerical results obtained from the FEM. Between experimental and FEM simulation of TD process, a good relationship was found.

**Keywords** Thermal drilling · Material flow · Temperature distribution · Optical microstructure · Simulation

## 1 Introduction

TD process is a bush-forming procedure beneficial towards thin sheet material for joints and tapping [1, 2]. In such processes, there is no material elimination takes place, and meanwhile, the bush or sleeve is formed from the base material. This process is also known as forming drilling, flow drilling, thermo-mechanical drilling, and friction drilling. In general, in TD process, the tungsten carbide material was employed as drilling tool. This process is completed with the consequent stages, as shown in Fig. 1. In the first stage, the drilling tool tip moves towards the workpiece, and therefore, it starts to penetrate into the workpiece. In the second stage, because of frictional effects, the high temperature is created at the contact zone.

Then, in the third stage, due to thermal energy, the workpiece becomes softened, and then, drilling tool penetrates smoothly down to produce the bushing around the drilled hole. At the fourth stage, the drilling tool returns towards starting position.

In this process, the workpiece material deformation is very high, and also generates high temperature at the interface of tool and workpiece [3–5]. For that reason, finite-element model is important to be familiar with the flow of deformed material, temperature distribution, stress, and strain rate, which is complicated to analyse experimentally in TD process. Miller et al. [6] developed semi-empirical analytical model according to contact pressure and temperature towards forecasting the thrust force and torque in TD process. This simplified analytical model is incapable to offer a detailed analysis of the deformation of workpiece material. The same author [7] studied the thermo-mechanical performance of TD process by the ABAQUS/EXPLICIT FEM software. In their investigation, they used 3D finite-element model since the deformation of the workpiece is in the rotational direction. Krasauskas et al. [8] performed experimental and finite-element analysis of TD of AISI 304 steel material. They examined the temperature distribution, torque and thrust force. Bilgin

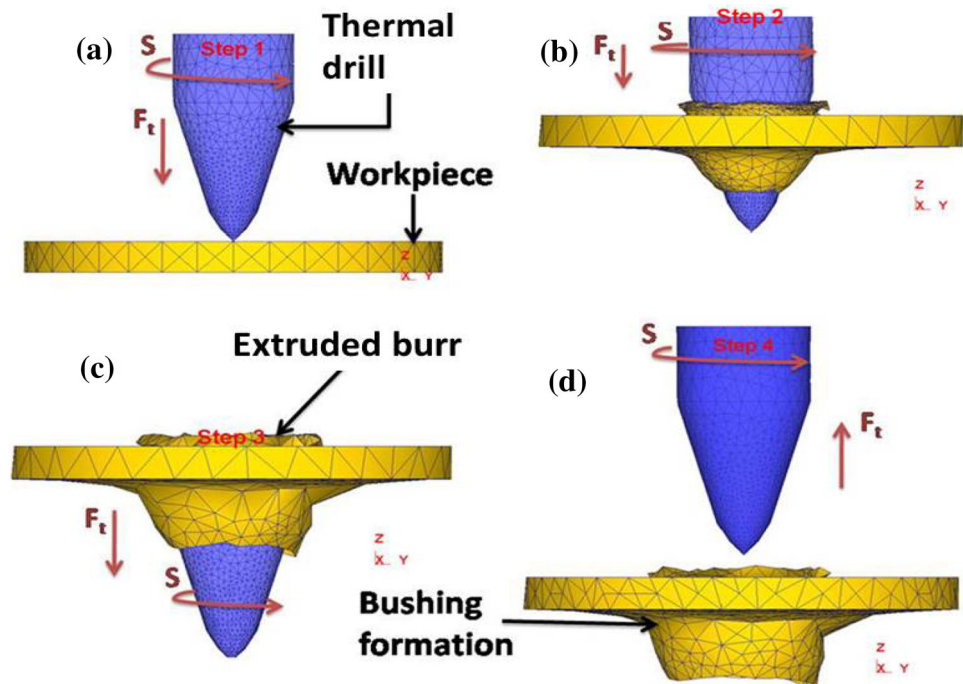
Technical Editor: Márcio Bacci da Silva.

✉ R. Kumar  
mepcokumar@gmail.com

N. Rajesh Jesudoss Hynes  
findhynes@yahoo.co.in

<sup>1</sup> Department of Mechanical Engineering, Mepco Schlenk Engineering College, Sivakasi, Tamilnadu 626005, India

**Fig. 1** Stages in thermal drilling  
**a** Step 1: centering. **b** Step 2:  
 piercing. **c** Step 3: bushing  
 formation. **d** Step 4: finishing



et al. [9] developed finite-element model by the DEFORM-3D software to compute the torque, thrust force, and heat transfer coefficients in the TD process of AISI 1020 steel. Miller et al. [10] carried out experiments on TD of Al 5052, titanium, AISI 1020 steel, and AISI 4130 steel and carefully studied about the microstructural changes during TD process. They reported that the microstructural changes happen due to the evolution of high temperature at frictional contact region that subsequently leads larger deformation in the thermally drilled holes in workpiece. Similar results were reported during experimental investigation on the modification of microstructure of thermal drilled Al 2024 alloy by Eliseev et al. [11]. The present work concentrates on the simulation of material flow and alterations of microstructure in TD process on GS sheet metal. The pattern of material flow in GS during TD process was studied using computation of the DEFORM-3D software through point-tracking technique.

## 2 Experimental methods

### 2.1 Material

In this work, GS workpiece was employed for TD process-based experimentation. GS was selected to be used as the workpiece in the present work, for the reason that it is used widely material in boat building, roofing material, door, and domestic appliances. The chemical composition of GS workpiece in weight percentage is 99.69% Fe, 0.003% C,

0.006% Si, 0.005% S, 0.018% P, 0.173% Mn, 0.011% I, 0.031 Cr, 0.001% Mo, 0.002% V, 0.017% Cu, 0.035% Al, 0.001% Nb, 0.004% Zn, and 0.05% Ti.

Tungsten carbide (WC) material was selected for thermal drill tool and it has the following dimensions such as diameter,  $d = 6$  mm; shank length,  $L_s = 20$  mm; shoulder length,  $L_{sh} = 8$  mm; cylinder length,  $L_{cy} = 15$  mm; conical length,  $L_{co} = 5$  mm; center length,  $L_{ce} = 2.5$  mm. The conical angles  $\phi$  is 45 degrees and center angle  $\Theta = 90^\circ$ . Thermal drill geometric and developed tool are shown in

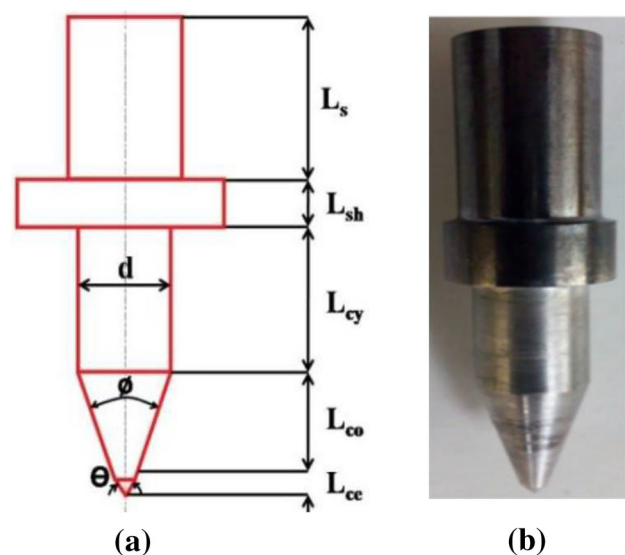


**Fig. 2** **a** Geometry of thermal drill. **b** Developed thermal drill

Fig. 2a, b, respectively. The properties of GS workpiece and tungsten carbide tool material are shown in Table 1.

### 2.2 Thermal-drilling (TD) processes

In this work, TD-drilling experiments were carried out on vertical drilling machine with 0.1–11 kW and 3 Phase Variable Frequency Drive. The schematic arrangement of TD process is shown in Fig. 3. The workpiece of GS has a cross-sectional dimension of 20 mm diameter and 2 mm thickness. The parameters involved in this work are displayed in Table 2. During the process, workpiece temperature was measured by non-contact-type Infrared Red thermometer (IRT). The workpiece temperature values for the period of the TD process were noted using IRT with the DATA TEMP MX software. Furthermore, microstructural characterization of thermal drilled GS workpiece was determined using de-winter inverted trinocular metallurgical microscope (DITMM) attached with 0.01 mm OCCULAR scale and has the magnification of 50×–1000×.

### 3 Finite-element simulation

The simulation method applied in this TD process is similar to the method typically used in friction stir spot welding (FSSW), because both TD and FSSW processes involve the similar working principle. That is in those processes, a rotating tool is employed to form the frictional contact and create high temperature at the interface. As a result, the joining of two materials in FSSW process and forming a hole in sheet metal in TD process will happen. This is the only one important dissimilarity which has to be followed in both FSSW and TD processes [7].

With the aim to simulate the TD process of GS workpiece, the DEFORM-3D software was chosen together with the formulation of Arbitrary Lagrangian–Eulerian (ALE). This is the finite-element method-based simulation software which is used to computing the different forming and

heat treatment problems in metal-forming operations and developed by the industries of scientific-forming technologies corporation. It has the ability to modeling and investigating of complex 3D material flow patterns. By the way of simulation of manufacturing process using computer, the designers or engineers become able to predict the material flow before experimental test leads to decrease the consumption of material and production costs. The succeeding assumption has been efficiently utilized in this simulation. They are: (a) thermal drill tool model is considered as rigid form; (b) workpiece model is considered as rigid visco-plastic form; (c) coefficient of friction at the interface is constant; and (d) heat losses due to radiation was small.

### 3.1 Governing equations

In this TD process, the thermo-mechanical analysis was successfully accomplished by solving the following continuity equation, momentum equation, and energy conservation equation together with properties of the material. According to normality principle, the mechanical property was designated [12]:

$$\delta_t = 2d_R\mu \tag{1}$$

$$d_R = \dot{\epsilon} \left[ \frac{\partial \bar{\sigma}_v}{\partial \delta_t} \right] = 1.5 \left[ \frac{\dot{\epsilon}}{\bar{\sigma}_v} \right] \delta_t = \delta_t / 2\mu \tag{2}$$

$$\bar{\sigma}_v = \sqrt{1.5\delta_t \cdot \delta_t}, \quad \dot{\epsilon} = \sqrt{0.6667d_R \cdot d_R} \tag{3}$$

where  $d_R$  is the deformation rate;  $\delta_t$  is the deviatoric stress tensors;  $\bar{\sigma}_v$  is the Von Mises yield stress;  $\dot{\epsilon}$  is the effective strain rate; and  $\mu$  is the viscosity. From Eqs. 1–3, the viscosity  $\mu(\dot{\epsilon}, T)$  is the function of strain rate  $\dot{\epsilon}$  and temperature  $T$  and the Von Mises yield stress  $\bar{\sigma}_v(T)$  is the function of temperature ( $T$ ):

$$\mu = 0.33 \left[ \frac{\bar{\sigma}_v}{\dot{\epsilon}} \right]. \tag{4}$$

According to conservation of momentum principle [12], the following equation (5) has been obtained as given below:

$$\nabla \cdot \sigma_c + \rho a = \rho \left[ \frac{dV}{dt} \right] \tag{5}$$

where  $\sigma_c$ ,  $\rho$ , and  $a$  are the Cauchy stress tensor, density, and acceleration, respectively;  $V$  and  $t$  are velocity vector and time, respectively, whereas  $d/dt$  is the derivative of material time as well as the density  $\rho(T)$  which is the function of temperature ( $T$ ).

The following equation (6) denotes the continuity equation [12] used for this process, where  $\partial/\partial t$  is derivative of spatial time:

$$V \cdot \nabla \rho = -\partial \rho / \partial t. \tag{6}$$

**Table 1** Thermal and mechanical properties of tungsten carbide and galvanized steel

Properties	Tungsten carbide	Galvanized steel
Melting point, °C	2870	1538
Thermal conductivity, W/m K	88	18
Poisson’s ratio	0.22	0.2
Young modulus, GPa	686	200
Shear modulus, GPa	283	78
Thermal expansion, 10 <sup>-6</sup> /K	7.1	6

**Fig. 3** Schematic diagram of thermal drilling process

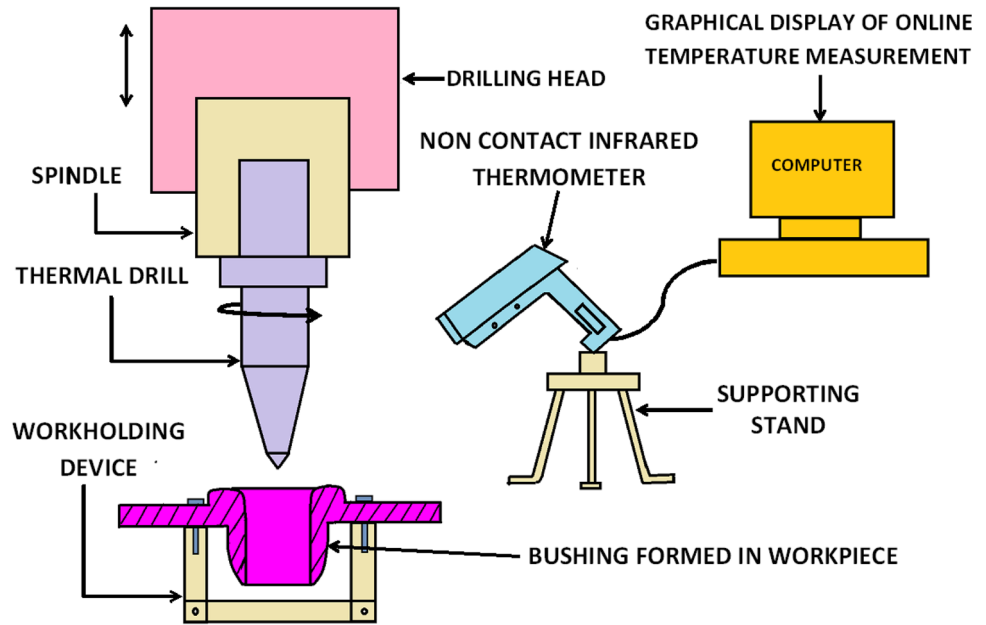


**Table 2** Thermal drilling process parameters

Process parameters	Values
Rotational speed, rpm	2400
Feed rate, mm/min	200
Tool angle, degree	45

Based on the law of energy conservation [12], the following equation (7) can be derived as

$$\rho c_s \frac{dT}{dt} = \nabla \cdot (K_t \nabla T) + \dot{q}_g \tag{7}$$

where  $c_s$  and  $K_t$  are the specific heat capacity and thermal conductivity, respectively;  $\dot{q}_g$  is the rate of heat generation; thermal conductivity  $K_t(T)$  is the function of temperature; and the subsequent equation (8) represents the heat generation rate  $\dot{q}_g$  [12], where  $C_f$  is the correction factor:

$$\dot{q}_g = C_f \delta_t \cdot d_R \tag{8}$$

The convective heat transfer coefficient  $h_c$  obtained by Eq. (7) is given below in Eq. (9), where  $T_s$  is the temperature of surroundings:

$$h_c = K_t \nabla T / (T - T_s) \tag{9}$$

### 3.2 Boundary conditions and mesh

To execute the TD process, the DEFORM-3D finite-element simulation software was used. Table 3 shows the simulation parameters used in this work. The workpiece model has the dimension of 20 mm diameter and 2 mm thickness. The model of the workpiece was made using the model creating features in the DEFORM-3D software. The

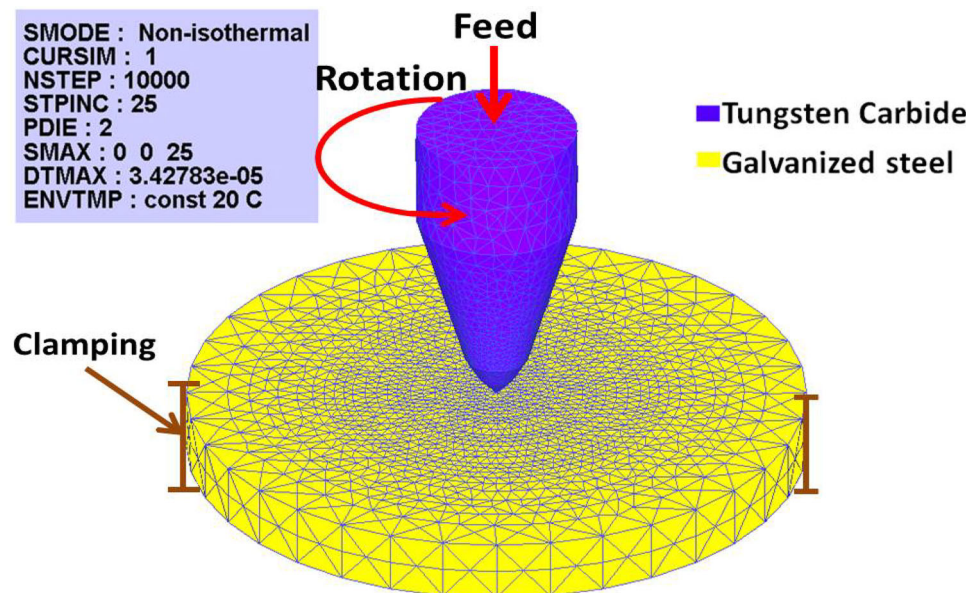
lateral surface of workpiece model was arrested in all X, Y, and Z directions to avoid the fluctuation during the simulation process. All surfaces of the workpiece and thermal drill model were under the boundary conditions of natural convection with  $20 \text{ W/m}^2 \text{ K}$ , shear friction factor at the tool, and workpiece was fixed at 0.6 and surrounding temperature of  $20 \text{ }^\circ\text{C}$ . However, the SOLIDWORKS 2014 modeling software was used to produce the STL format file of 3D geometric model of thermal drill, and then, this model was imported into the program of the finite-element DEFORM-3D software. The materials designated for finite-element models of thermal drill tool and workpiece were tungsten carbide and GS workpiece, respectively. The thermal drill tool was modelled as a rigid body, because it is not for the determination of stress and strain rate. The workpiece was modelled as a rigid visco-plastic body.

The process of meshing is implemented for finite-element simulation. The tetrahedral element mesh structure is selected for these models. Workpiece mesh structure contains 25,071 elements and 8450 nodes and tool mesh structure contains 10,826 elements and 5541 nodes. The mesh size ratios of 0.2 and 0.1 were selected for thermal drill tool model and workpiece model, respectively. The assembled mesh structure of tool and workpiece is shown in Fig. 4. As shown in Fig. 4, rotational speed (S) 2400 rpm on its Z-axis and feed rate ( $F_t$ ) 200 mm/min in the same direction were applied towards thermal drill tool model.



**Table 3** Simulation parameters used in the DEFORM-3D Software

Parameters	Conditions
Rotational spindle speed, $S$	2400 rpm
Feed rate, $F$	200 mm/min
Shear friction factor	0.6
Workpiece shape and conditions	Cylinder and fixed at lateral surfaces
Room temperature	20 °C
Workpiece shape	20 mm diameter, 2 mm thick
Tool type, shape	Rigid, conical
Mesh generation method	Adaptive mesh
Mesh size ratio of workpiece and tool	0.1 and 0.2
Simulation controls	Lagrangian incremental Simulation steps—10,000 Step increment to save—25 Sparse solver

**Fig. 4** Mesh and boundary conditions

## 4 Results and discussion

### 4.1 TD material flow appearances

During the course of TD process, the identity of the movement of workpiece material is challenging by the conventional analytical approach, because it is directly influenced by the effect of rotational speed and feed rate. Therefore, by knowing alterations in the physical structure of the material in TD process, it is important to select the parameters such as rotational speed and feed rate for TD process. The DEFORM-3D simulation software is capable to visualize the pattern of flow happening in this process. The workpiece material flow in TD process could be examined effectively by the way of point-tracking technique [13, 14]. The nine tracer points were set at the region

of TD process in the workpiece material. These points were used to find the movement of material during the period of the drilling process. Figure 5 shows the numbering of nine tracer points which was assigned the number from 1 to 9. First, locate the three trace points  $P1-P3$  on the drilling zone Z-axis line with an incremental depth of 1 mm from the upper surface of workpiece towards the downward direction. Then, locate the trace points  $P4-P6$  and  $P7-P9$  at the distance of 1 mm from the central axis ( $X0$ ,  $Y0$ , and  $Z0$ ). Table 4 shows the coordinate points for  $P1-P9$  used in this simulation study of TD process. Rotational speed and feed rate of the thermal drill are set as the following values such as 2400 rpm and 200 mm/min, respectively. 2 mm thickness GS workpiece is used for this analysis. At the initial stage, the thermal drill just comes into touch with the upper surface of the workpiece. As a result, there is no

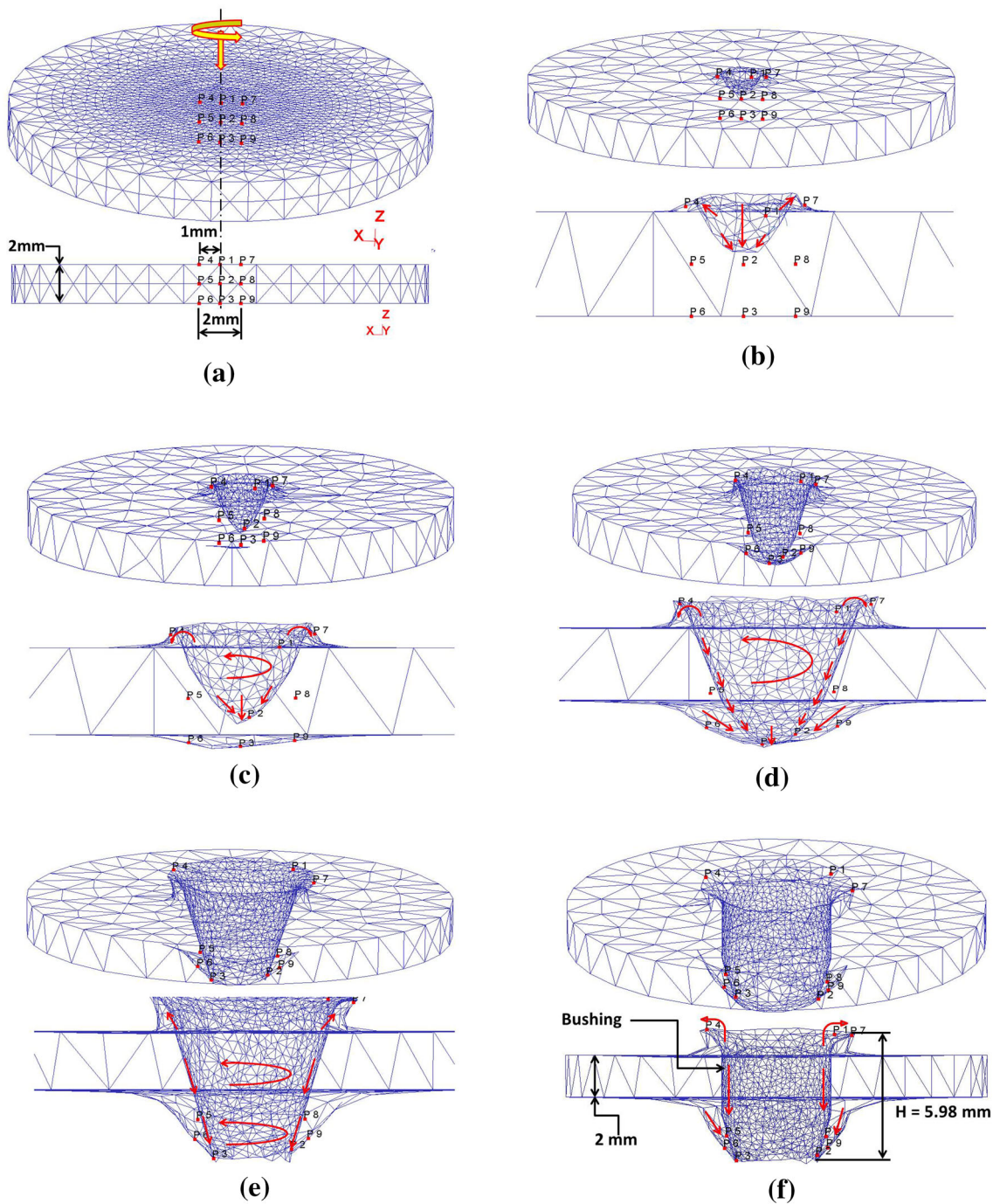


**Fig. 5** a Initial points' position on the thermal drilling zone designated for material flow analysis. b Material flow during piercing of center zone of thermal drill. c Separation of lower surface of galvanized steel. d Material flow during piercing of conical zone of

material flow happens at this stage, as shown in Fig. 5a. Then, in the second stage, the thrust force plays the main role, while the center zone of drill penetrates into the workpiece. Consequently, the upper portion of GS workpiece is compressed ahead at this stage and leads to move downward. The upper tracer points *P4*, *P1*, *P7*, *P2*, and *P3*

thermal drill. e Material flows during formation of hole in galvanized steel. f Final position of points after formation of bushing around the hole in galvanized steel

are displaced from the initial position, which is displaced in Fig. 5b, c. At the moment, Point *P4* and *P7* jumps to move upward and center point *P1* commences fast to rotate with the drill as well as *P2* and *P3* also goes downward. Meanwhile, friction force at the interface of drill and GS generates red hotness at the center point *P1*. Subsequently,

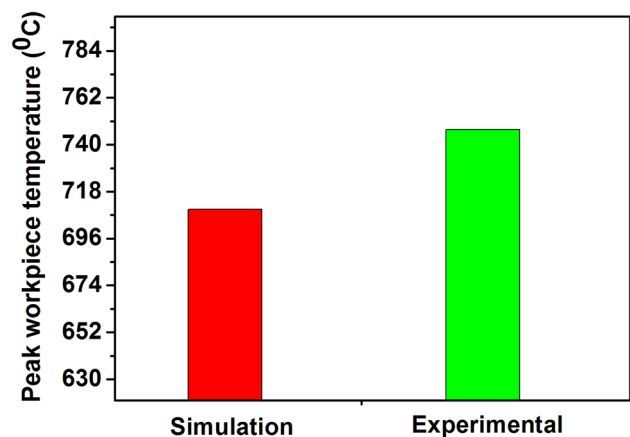
**Table 4** Location of tracer points in GS workpiece model

Tracer points	Locations of points		
	X-axis	Y-axis	Z-axis
1	0	0	0
2	0	0	- 1
3	0	0	- 2
4	1	0	0
5	1	0	- 1
6	1	0	- 2
7	- 1	0	0
8	- 1	0	- 1
9	- 1	0	- 2

in the third stage, the conical zone penetrates into the workpiece after passing of center zone of drill thoroughly. Figure 5d, e illustrates the entering of the conical zone of the drill into the workpiece. Due to the more frictional heat generation, softening at the drilling zone and the conical zone pierces effortlessly. In this stage, separation of galvanized material occurs owing to produce a hole. By way of increasing of workpiece temperature under this circumstance, there is a greater trend to attain the plastic deformation. The points *P2* and *P3* are displaced in this stage with not merely compression force in *Z*-direction, but also due to the rotation with the action of shear force in both *X* and *Y* directions. At that time, the points *P3* and *P2* shifted apart a distance of diameter of the conical zone and Fig. 5e demonstrates the formation of a hole in the workpiece at the end of this stage. Afterwards, in the final stage, the cylindrical zone of thermal drill enters into the workpiece after completely passing through the conical zone. The points *P5*, *P6*, *P3*, *P8*, *P9*, and *P2* are shifted in the lower surface of the workpiece, which is around the thermal drill with almost identical conical zone diameter. The points *P4*, *P1*, and *P7* turn in the extended burr of the workpiece; those points are positioned around the cylindrical zone of the thermal drill. Finally, the bush like shape is formed in the drilling zone, which is shown in Fig. 5f. The height of bushing formed by the simulation model in the workpiece of GS is 5.98 mm. As a result, the height is almost three times higher than the thickness of GS workpiece (2 mm). The experimental by an obtained value of bushing is 5.94 mm; when it is compared with the simulation result, minimum error of less than  $\pm 1\%$  has been observed.

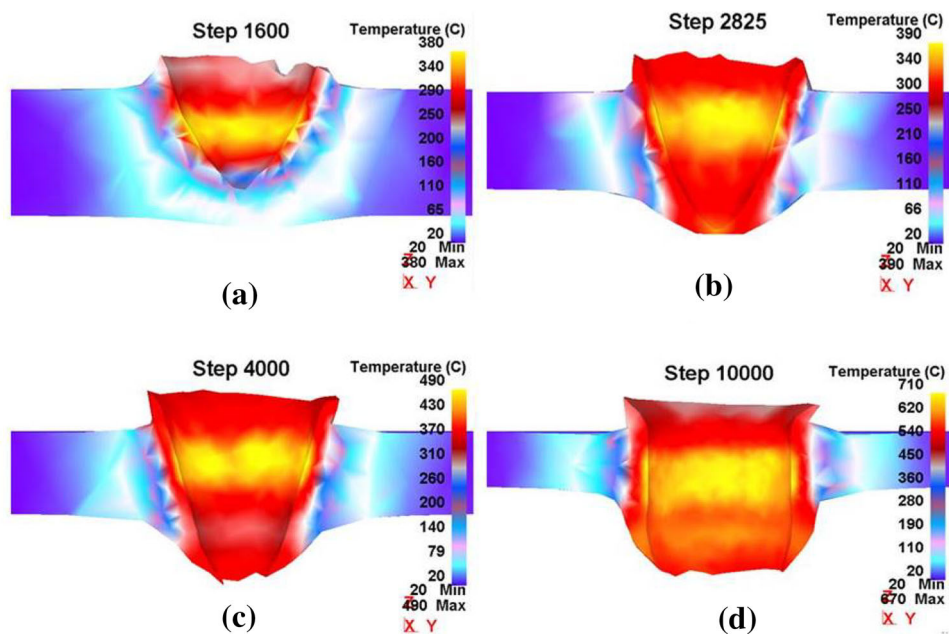
## 4.2 Finite-element model validation

The validation of simulation results is essential with the aim to confirm the accuracy of this model. Therefore, it is substantial to validate it by means of comparing this simulation result with the experimental result. Using the peak temperature occurred during TD process on GS workpiece as a basis the finite-element simulated model is confirmed. By this way in Fig. 6, the predicted peak temperature (709.71 °C) by simulation was compared with the experimental peak temperature (747.12 °C) which is recorded using IRT with the DATA TEMP MX software. During the process of TD, the material in the inner surface reaches visco-plastic stage due to frictional heating between the tool and the workpiece. In the first few seconds, of the initial stage of TD process, the material in the inner region of the workpiece is heated and it flows out in the form of red hot extended burr at the top surface. Since the infrared thermometer focussed on this extended burr region which was being expelled over the top surface, it records the peak temperature value (747.12 °C) as high as the peak temperature value predicted by the simulation software at the inner region (709.71 °C). It has been observed that both the simulated and experimental values have a high degree of closeness with a deviation  $\pm 5.27\%$ . Deviation of simulation results from experimental results may be attributed to the assumptions made in numerical modeling. The simulation model result of temperature distribution during the various stages of TD process is shown in Fig. 7. The prediction of peak temperature distributed inside the hole, while TD process occurred at the various simulation steps such as 1600, 2825, 4000, and 10,000 are 380, 390, 490, and 710 °C are simulated and studied.

**Fig. 6** Validation of simulation and experimental result



**Fig. 7** Temperature distributions



### 4.3 Microstructural investigation

Thermal drilled GS workpiece was mounted on Bakelite, and then, burrs are removed by means of polishing. Then, workpiece fixed on Bakelite is placed over the rotating disc of the polishing machine. Polishing operation was carried with very fine flaky powder for 3 min. Approximately 0.025 mm of workpiece material was detached. Using metallurgical microscope at 100 $\times$  magnification, the microstructure of thermal drilled GS material was analysed. Under the processing conditions of 2400 rpm, rotational speed and 200 mm/min feed rate. Figure 8a shows the cross-sectional view of thermal drilled GS. The microstructure of the GS before TD process is given in Fig. 8b. Non-equiaxed grains are observed in the parent material before TD process. During TD process, because of the heat, input recrystallization of grains is observed, as shown in Fig. 8c. Closely packed equiaxed grains are observed. Furthermore, heating during the process results in reduced grain structure, as shown in Fig. 8d. Inward grain flow is visible in Fig. 8e, f, as well as fibre lines that are stream lined along the direction of the axial movement of the tool. Due to rotational speed 2400 rpm, the intense heat is produced at the interface of thermal drill and GS workpiece. This was enough to increase the temperature of GS workpiece to its plastic state and become softer. Due to stirring action of the thermal drill, while the center region enters into the GS material, the recrystallization phenomenon [15] happens in that region. After piercing of center region, the conical and cylindrical regions of the thermal drill were entering into the GS material; the grain structure was elongated towards the downward direction.

Furthermore, TD process causes austere plastic deformation of GS workpiece and leads to produce high temperature. As a result of high drilling temperature (747.12  $^{\circ}$ C), zinc in the GS workpiece gets evaporated at 420  $^{\circ}$ C from the drilling zone [16]. The micrographs from Fig. 8c–f show the alternation in grain structure of GS workpiece due to the reason of heat generation during the process. While the GS workpiece material is heated to peak temperature, the rearrangement of carbon particles takes place. Consequently, after drilling process, while the GS drilled hole was cooled, the ferrite structure is produced. The allotriomorphic ferrite [17] was formed as a consequence of 2400 rpm rotational speed and the similar trend was observed in all the micrographs of thermal drilled GS workpiece.

## 5 Conclusions

In this present investigation, three-dimensional thermo-mechanical coupled simulation model of TD process on GS workpiece has been successfully established and compared with the experimental value. The significant outcomes could be summarized as follows:

1. The peak workpiece temperature is effectively correlated between the finite-element simulation results (709.71  $^{\circ}$ C) and experimental results (747.12  $^{\circ}$ C) during TD process on GS workpiece. The obtained peak temperature is approximately 0.56 times the melting temperature of GS workpiece.



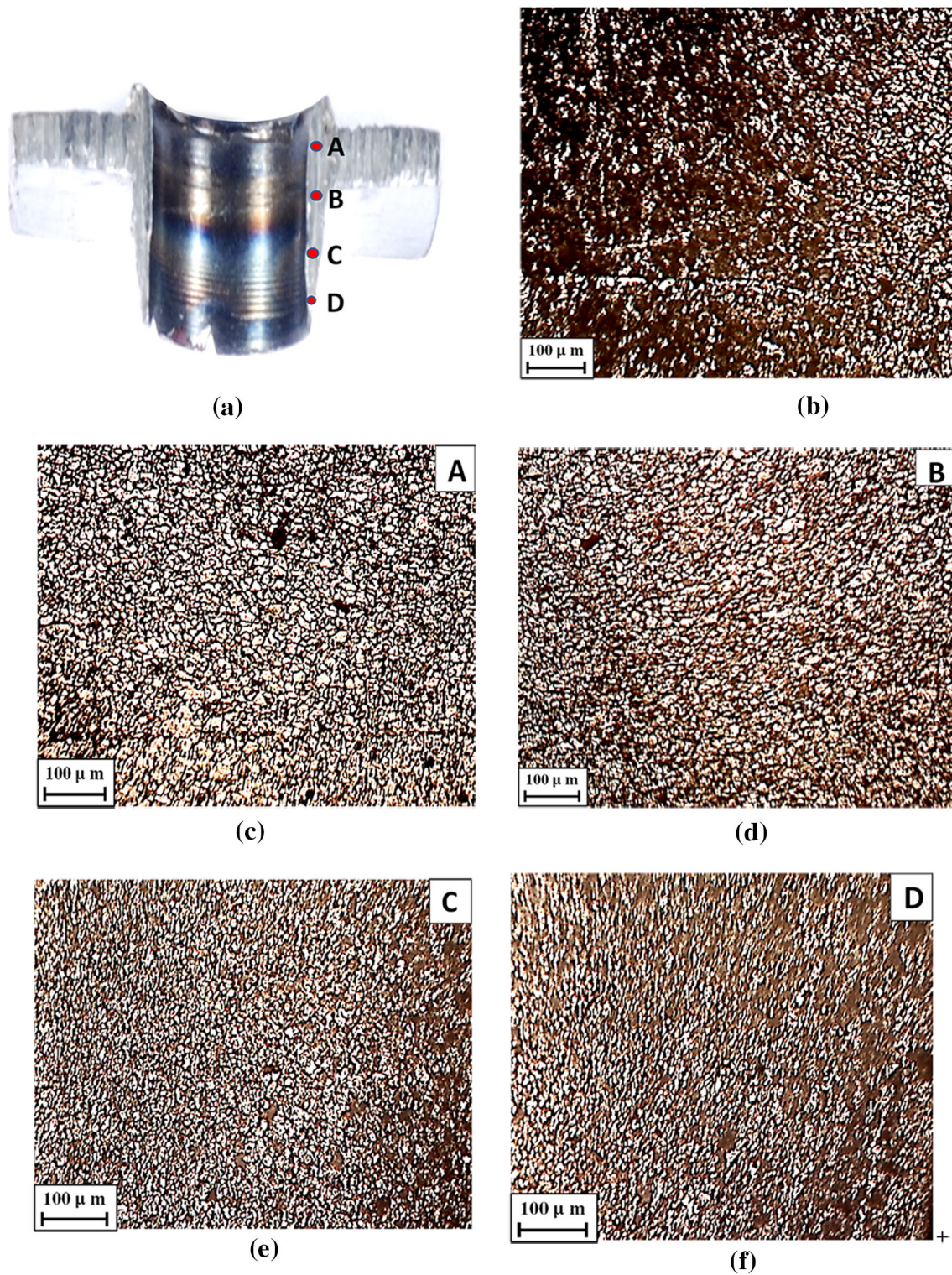


**Fig. 8** **a** Cross-sectional view of thermal drilled galvanized steel. **b** Optical microstructure of GS workpiece before thermal drilling. **c** Optical microstructure at A. **d** Optical microstructure at B. **e** Optical microstructure at C. **f** Optical microstructure at D

2. The results of point tracking technique ( $P1$ ,  $P2$ ,  $P3$ ,  $P4$ ,  $P5$ ,  $P6$ ,  $P7$ ,  $P8$ , and  $P9$ ) precisely validate the bushing shape in the drilled zone. The upper surface

material is moved partially upward and downward at the moment of stirring of the thermal drill in GS

- workpiece. The movement of lower surface material is displaced downward to form the bush around the hole.
- Bushing length of simulation model (5.98 mm) is fabulously correlated with the experimental bushing length value (5.94 mm) under the condition of TD process such as 2400 rpm rotational speed and 200 mm/min feed rate. Hence, this simulation model is validated with the experiment of TD process on GS workpiece.
  - The optical microstructural investigation on cross-sectioned thermal drilled workpiece of GS workpiece is studied efficiently.

## References

- Ozler L, Dogru N (2013) An experimental investigation of hole geometry in friction drilling. *Mater Manuf Process* 28:470–475. <https://doi.org/10.1080/10426914.2012.746699>
- Ku WL, Hung CL, Lee SM, Chow HM (2011) Optimization in thermal friction drilling for SUS 304 stainless steel. *Int J Adv Manuf Tech* 53:935–944. <https://doi.org/10.1007/s00170-010-2899-5>
- Hynes NRJ, Kumar R (2017) Process optimization for maximizing bushing length in thermal drilling using integrated ANN-SA approach. *J Braz Soc Mech Sci Eng*. <https://doi.org/10.1007/s40430-017-0820-y>
- Hynes NRJ, Maheshwaran MV (2016) Numerical analysis on thermal drilling of aluminum metal matrix composite. *AIP Conf Proc* 1728:1–4. <https://doi.org/10.1063/1.4946597>
- Raju BP, Kumaraswamy M (2012) Finite element simulation of a friction drilling process using deform-3D. *Int J Eng Res App* 2(6):716–721
- Miller SF, Wang H, Li R, Shih AJ (2006) Experimental and numerical analysis of the friction drilling process. *J Manuf Sci Eng* 128(3):802–810. <https://doi.org/10.1115/1.2193554>
- Miller SF, Shih AJ (2007) Thermo-mechanical finite element modeling of the friction drilling process. *J Manuf Sci Eng* 129:531–538. <https://doi.org/10.1115/1.2716719>
- Krasauskas P, Kilikevičius S, Česnavičius R, Pačenga D (2014) Experimental analysis and numerical simulation of the stainless AISI 304 steel friction drilling process. *Mecha* 20(6):590–595. <https://doi.org/10.5755/j01.mech.20.6.8664>
- Bilgin MB, Gok K, Gok A (2015) Three-dimensional finite element model of friction drilling process in hot forming processes. *Proc IMechE Part E* 231(3):548–554. <https://doi.org/10.1177/0954408915614300>
- Eliseev AA, Fortuna SV, Kolubaev EA, Kalashnikova TA (2017) Microstructure modification of 2024 aluminum alloy produced by friction drilling. *Mater Sci Eng A* 691:121–125. <https://doi.org/10.1016/j.msea.2017.03.040>
- Miller SF, Blau P, Shih AJ (2005) Microstructural alterations associated with friction drilling of steel, aluminum, and titanium. *J Mater Eng Perform* 14(5):647–653. <https://doi.org/10.1361/105994905X64558>
- Kim D, Badarinarayan H, Ryu I, Kim JH, Kim C, Okamoto K, Wagoner RH, Chung K (2010) Numerical simulation of friction stir spot welding process for aluminum alloys. *Met Mater Int* 16(2):323–332. <https://doi.org/10.1007/s12540-010-0425-9>
- Zinati RF, Razfar MR (2015) Finite element simulation and experimental investigation of friction stir processing of polyamide 6. *Proc IMechE Part B* 229(12):2205–2215. <https://doi.org/10.1177/0954405414546705>
- Pashazadeh H, Masoumi A, Teimournezhad J (2013) A study on material flow pattern in friction stir welding using finite element method. *Proc IMechE Part B* 227(10):1453–1466. <https://doi.org/10.1177/0954405413485952>
- Baek SW, Choi DH, Lee CY, Ahn BW, Yeon YM, Song K, Jung SB (2010) Microstructure and mechanical properties of friction stir spot welded galvanized steel. *Mater Trans* 51(5):1044–1050. <https://doi.org/10.2320/matertrans.M2009337>
- Vináš J, Kaščák L, Greš M (2016) Optimization of resistance spot welding parameters for microalloyed steel sheets. *Open Eng* 6:504–510. <https://doi.org/10.1515/eng-2016-0069>
- Mazzaferro CCP, Rosendo TS, Tier MAD, Mazzaferro JAE, Santos JFD, Strohaecker TR (2015) Microstructural and mechanical observations of a galvanized trip steel after friction stir spot welding. *Mater Manuf Process* 30(9):1090–1103. <https://doi.org/10.1080/10426914.2015.1004699>